ELSEVIER

International Journal of Heat and Fluid Flow 22 (2001) 603–613

International Journal of HEAT AND FLUID FLOW

www.elsevier.com/locate/ijhff

# Experimental study of developing turbulent flow and heat transfer in ribbed convergent/divergent square ducts

Liang-Bi Wang [a,1], Wen-Quan Tao [a,*], Qiu-Wang Wang [a], Tsun Tat Wong [b]

[a] School of Energy and Power Engineering, Xi'an Jiaotong University, Xi'an, Shaanxi 710049, China
[b] Department of Mechanical Engineering, Hong Kong Polytechnic University, Kowloon, Hong Kong, China

Received 22 September 2000; accepted 8 June 2001

**Abstract**

The local heat transfer and pressure drop characteristics of developing turbulent flows of air in three stationary ribbed square ducts have been investigated experimentally. These are: ribbed square duct with constant cross-section (straight duct), ribbed divergent square duct and ribbed convergent square duct. The convergent/divergent duct has an inclination angle of 1°. The measurement was conducted within the range of Reynolds numbers from 10 000 to 77 000. The heat transfer performance of the divergent/convergent ducts is compared with the ribbed straight duct under three constraints: identical mass flow rate, identical pumping power and identical pressure drop. Because of the streamwise flow acceleration or deceleration, the local heat transfer characteristics of the divergent and convergent ducts are quite different from those of the straight duct. In the straight duct, the fluid flow and heat transfer become fully developed after 2–3 ribs, while in the divergent and convergent ducts there is no such trend. The comparison shows that among the three ducts, the divergent duct has the highest heat transfer performance, the convergent duct has the lowest, while the straight duct locates somewhere in between. 

## 1. Introduction

Turbulent heat transfer and fluid flow characteristics of air in rib-roughened tubes, annuli, ducts and between parallel plates have been studied extensively because of their important applications. Such a heat transfer enhancement method is widely used in cooling passages of gas turbine blade, compact heat exchangers, fuel elements in advanced gas-cooled reactor, electronic cooling devices, etc. Taking the cooling passages of gas-turbine blade as an example, the internal cooling passages are usually approximated by a rectangular duct with a pair of opposite rib-roughened walls (Han and Park, 1998). The present investigation was mainly motivated to investigate the cooling technique of a gas-turbine blade, therefore in the following review the references mentioned are mainly related to this subject.

In the experimental investigations reported in the literature, the internal cooling passages of a gas turbine have been modeled by either square or rectangular channels having two opposite walls equipped with turbulence promoters. The effects of such geometric parameters as the relative rib height, relative rib pitch, attack angle, duct aspect ratio, rib cross-section geometry, and rib configuration (straight or v-shape; continuous or discrete) have been widely studied. The following is only a brief review of partial works. One of the earliest experimental data was reported by Burggraf (1970), who studied the turbulent air flow in a square duct with two opposite ribbed walls. Han et al. (1978) conducted a systematic investigation of the heat transfer and friction losses in rib-roughened surface. Metzger et al. (1998) investigated the effect of various rib configurations in a rectangular duct. Han and Lei (1983), Han (1984) and Han et al. (1985) conducted tests in a square duct and developed correlations to predict the friction factor and average Stanton number in the fully developed region as a function of the flow characteristics and the geometric parameters of the passage and turbulence promoter. Taslim and Spring (1987, 1988, 1991) studied the effect of passage aspect ratio and various rib geometries. Lau et al. (1991) performed an experimental work to study the effects of different distributions of the rib on the fully developed heat transfer, including the 90° transverse rib, 90° discrete ribs, parallel and crossed oblique discrete ribs with different attack angles. Several studies on developing turbulent flow and heat transfer have also been reported in Metzger et al. (1998) and Han and Park (1988). In Han and Park (1988) the combined effects of the rib angle and the channel aspect ratio on the distribution of the local heat transfer coefficient for the developing turbulent heat transfer in short rectangular channels ($L/D_h = 10$ and 15) with a par of opposite rib-roughened walls were measured. It was found that in the square channel with 90° rib angle, the periodic Nusselt number decreases in the streamwise direction

* Corresponding author. Tel.: +86-029-2669106; fax: +86-029-3237910.
*E-mail address:* wqtao@xjtu.edu.cn (W.-Q. Tao).
[1] Present address: Department of Mechanical Engineering, Lan Zhou Railway Institute, Lan Zhou 730070, China.

0142-727X/01/$ - see front matter 
PII: S0142-727X(01)00127-8

**Nomenclature**

| | |
|---|---|
| $A$ | surface area, $m^2$ |
| $A(x)$ | surface area from inlet to the position of $x$, $m^2$ |
| $c_p$ | heat capacity, J/kg K |
| $C_p$ | pressure recovery factor |
| $d_1, d_2$ | depth of ditch |
| $D_h$ | hydraulic diameter |
| $D_m$ | average hydraulic diameter, m |
| $e$ | rib height, m |
| $f$ | friction factor |
| $h$ | heat transfer coefficient, $W/m^2$ K |
| $k$ | thermal conductivity, W/m K |
| $l_1, l_2$ | length of ditch with different depths |
| $L$ | axial length of duct, m |
| $\dot{m}$ | mass flow rate, kg/s |
| $Nu$ | Nusselt number |
| $Nu_s$ | Nusselt number of smooth side |
| $Nu_r$ | Nusselt number of ribbed side |
| $Nu_t$ | duct average Nusselt number |
| $p$ | pressure, Pa; spacing between two neighboring ribs, m |
| $\Delta p$ | pressure drop of duct, Pa |
| $Q$ | heat transfer rated, W |
| $Q_{loss}$ | heat loss to the environment, W |
| $Re$ | Reynolds number |
| $Re_m$ | Reynolds number based on $D_m$ |
| $T$ | temperature, K |
| $T_w$ | wall temperature, K |
| $U$ | cross-section average streamwise velocity, m/s |
| $x$ | streamwise direction |

*Greeks*

| | |
|---|---|
| $\lambda$ | parameter defined by Eq. (13) |
| $v$ | kinetic viscosity, $m^2/s$ |
| $\rho$ | fluid density, $kg/m^3$ |

*Subscripts*

| | |
|---|---|
| b | bulk |
| in | inlet |
| m | mean |
| x | local |
| out | outlet |

from the sharp entrance and then reaches a constant periodic distribution after $x/D_h > 3$. Apart from the conventional heat transfer measurement method, the heat/mass transfer analogy method and the optical method also have been extensively used. Lockett and Collins (1990) conducted the double exposure holographic interferometry measurement for a fully developed heat transfer in a parallel channel with square and rounded rib roughness on one wall. Similar holographic investigation was conducted by Liou et al. (1993) for the periodic fully developed heat transfer in parallel channel. As far as the mass/heat transfer analogy is concerned, the naphthalene sublimation technique was used quite often. Sparrow and Tao (1983, 1984) adopted this technique to study the developing and developed heat transfer characteristics for rectangular ducts with rods on one and two principal walls. Later a lot of investigations using this technique were conducted, among which the work performed by Chyu and Naturajan (1995) is mentioned here, in which the local heat transfer characteristics of a three-pass smooth and turbulated passage were modeled. To simulate the actual passage geometry, the test model had a trapezoidal cross-section with streamwise variable passage sizes. Abuaf and Kercher (1994) using the liquid crystal technique measured the three-pass turbulated passage. The model closely duplicated the blade's leading edge, mid-chord and trailing edge cooling passage geometries with streamwise varying cross-sectional area. The above brief review shows that the transport phenomenon inherited in such a complex configuration represents one of the most challenging issues in the study of heat transfer enhancement.

As presented in Abuaf and Kercher (1994), Medwell et al. (1991), in typical airfoils with multipass cooling circuits, the cross-sectional area of radial passage usually varies along the passage from root to tip. In other words, the cooling passages are actually convergent or divergent to some extent. Such a geometric variation may induce substantial difference in both flow and heat transfer characteristics compared to those models with straight rectangular channel.

However, no significant study was found in the existing literature that deals with heat transfer in ribbed roughened convergent/divergent ducts. Wang et al. (2001) found that for a smooth square duct a mild streamwise variation of cross-sectional area may induce significant difference in the local and average heat transfer behaviors. It is thus the objective of the present study to discern the flow and heat transfer characteristics in ribbed convergent and divergent square ducts. In the study, an experimental measurement was conducted to find the developing heat transfer and friction characteristics of turbulent flow in ribbed convergent and divergent stationary square ducts with uniform heat flux boundary condition. The heat transfer characteristics of a ribbed square straight duct were also measured. Thermal performance comparison among the straight, convergent and divergent ducts was conducted under three constraints (identical pumping power, identical pressure loss and identical mass flow rate).

## 2. Experimental apparatus

A schematic of the experimental system is shown in Fig. 1. This is an open test loop, with the room air being drawn by a 3.5 kW blower situated at the downstream end of the test loop. The forced air goes through an entrance section, a pre-plenum (square duct with $120 \times 120$ $mm^2$ cross-section), a test section, an after-plenum ($120 \times 120$ $mm^2$ square duct) and a 60 mm diameter, 1440 mm length pipe, equipped with a multiport averaging Pitot tube to measure the flow rate (Miller, 1996). A pre-plenum between the entrance section and the test section is employed to provide a sharp constriction for the air entering the test section. This entrance condition is believed to be more realistic than the inlet with gradually varying cross-section.

Both uniform square ribbed and convergent/divergent square ribbed ducts are studied. The ribs are manufactured as integral parts on two opposite walls of the duct. The uniform square duct has a cross-section of $50 \times 50$ $mm^2$. The convergent/divergent square ribbed duct has the largest cross-section of $58 \times 58$ $mm^2$ and the smallest cross-section of $41 \times 41$ $mm^2$. Each test duct is 500 mm long. This geometry makes the convergent/divergent duct having 1° inclination along the two directions in the cross-section. The ribbed square duct with uniform cross-section (straight duct) and the divergent/convergent ducts are schematically presented in Figs. 2(a) and (b), and the inclination of the duct is shown in Fig. 2(c). As shown in Fig. 2, the same duct was used either as convergent or di-

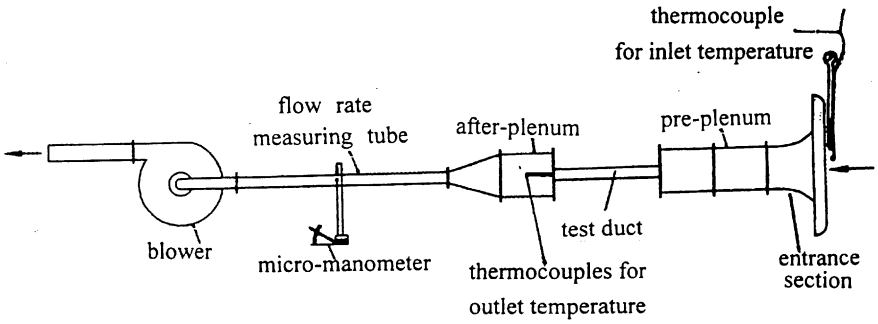


Fig. 1. Schematic diagram of test apparatus.

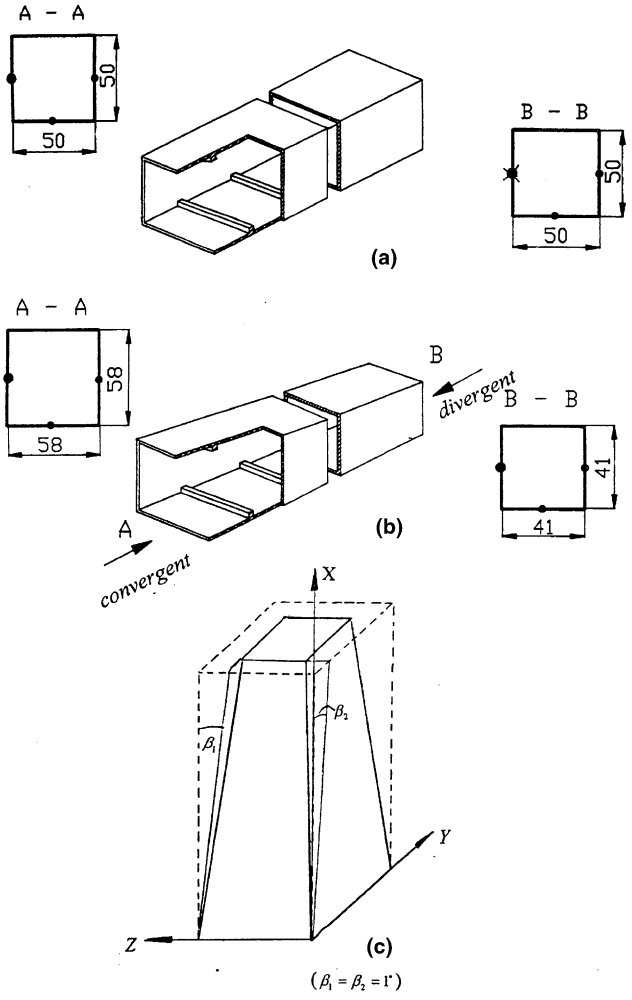


Fig. 2. Diagram of test tube: (a) ribbed duct of constant cross-section; (b) ribbed divergent/convergent duct; (c) schematic diagram showing the inclination angle.

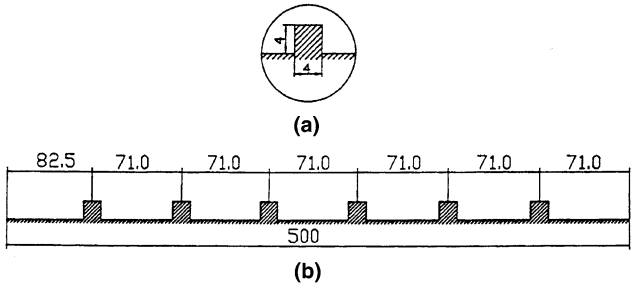


Fig. 3. Rib size and arrangement: (a) rib size; (b) rib arrangement.

vergent one, depending on the flow direction. The two small black circles shown in Figs. 2(a) and (b) represent the locations of the thermocouples and the big black one stands for the location of pressure tap.

The rib size and arrangement are presented in Fig. 3 with a fixed $e/D_m = 0.081$ and $p/e = 17.8$, where $D_m$ is the duct average value of hydraulic diameter. To get a detailed distribution of the local heat transfer coefficient, 120 thermocouples are imbedded in one of the ribbed walls along its centerline to measure the surface temperatures. The thermocouple arrangement is presented in Fig. 4, where Fig. 4(a) presents the details from the inlet to the first rib, while Fig. 4(b) gives the thermocouple locations between two subsequent ribs. In addition, 45 thermocouples are employed to measure the temperature distribution of one smooth wall. The details of the thermocouple locations on the smooth wall are shown in Fig. 4(c) (from the inlet to the position of first rib on the ribbed surface) and Fig. 4(d) (between two adjacent ribs). On the opposing smooth wall, 21 pressure taps are set up along the wall centerline. The axial arrangement of the pressure tap is presented in Fig. 4(e). It is to be noted that in order to measure the pressure drop across one cycle, the tap locations are repeated from cycle to cycle.

The details of the thermocouple setup are now described. As shown in Fig. 5(a), at the inner surface of one principal wall, 120 parallel ditches with width $w$ were first made in the half part of the surface. The depth of each ditch is shown in Fig. 5(b), where it can be seen that about 5 mm ditch ($l_1$) has a depth of 0.25 mm and the other part of the ditch ($l_2 \approx 5$ mm) has a depth of 0.75 mm. The hot junction of each thermocouple was imbedded at the end of the shallow ditch, while the two pieces of leading wire, which were coated by insulating lacquer, were drawn successively along the shallow and deep ditches outside the surface. Each ditch was then filled up with tin. The upper surface of each ditch was polished by sandpaper such that the entire inner surface can be regarded as an integrated smooth one. The ditch width, $w$, was about 1.2 mm, and the distance between two neighboring ditches, $s$, was limited by conditions in machining and setup of the thermocouple. The smallest value of $s$ in this study was 3 mm.

The test ducts were wrapped uniformly by a resistance strip which was controlled by a variac transformer to provide a controllable electrical heating to the test duct. The ducts are well insulated by an insulation material. The test duct wall was made of low-carbon steel. The wall thickness was 2 mm. For

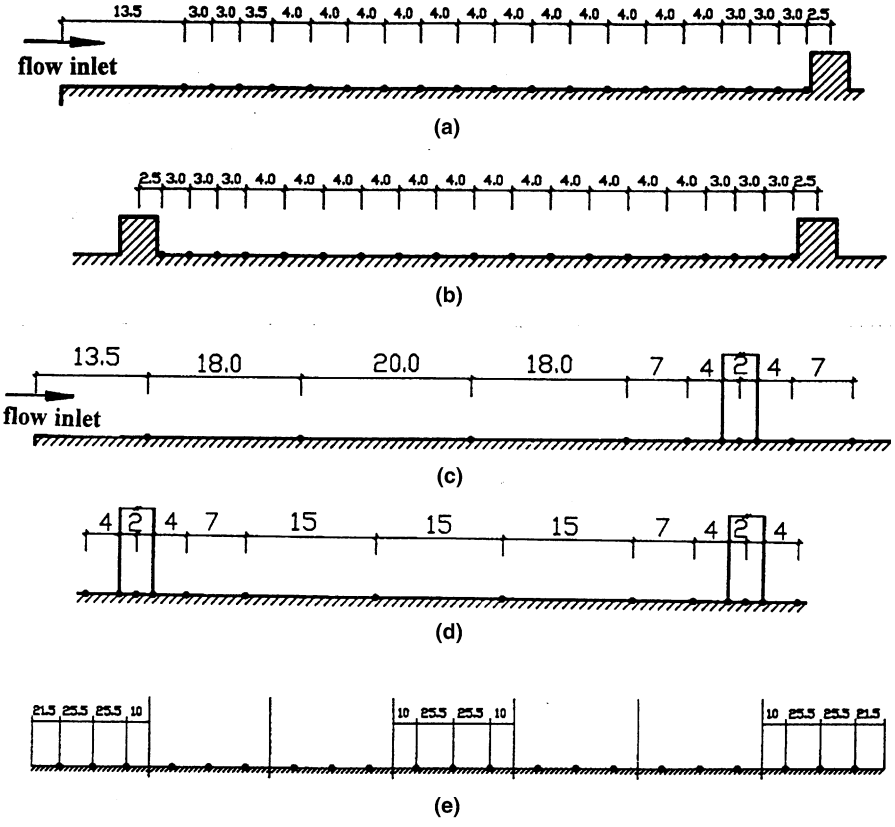


Fig. 4. Thermocouple and pressure tap distribution: (a) rib-side thermocouple distribution (from inlet to first rib); (b) rib-side thermocouple distribution (between two subsequent ribs); (c) smooth surface thermocouple distribution (from inlet to the first rib of ribbed surface); (d) smooth surface thermocouple distribution (betwen two subsequent ribs); (e) pressure tap distribution.

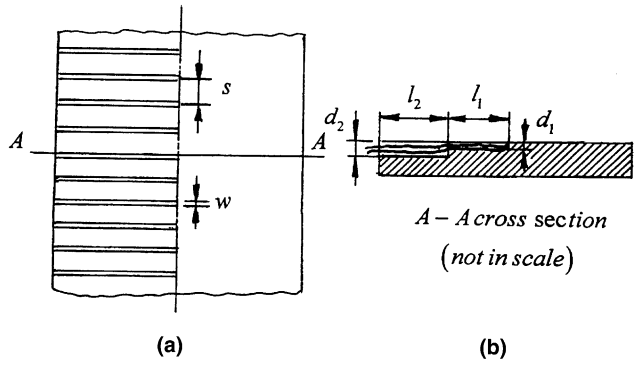


Fig. 5. Details of thermocouple setup.

all the test cases, the maximum wall temperature was less than about 90 °C, and the maximum temperature drop between the duct outlet and the duct inlet was less than about 50 °C. The mean bulk temperature of the fluid in the duct varied from 30 to 50 °C. The thermal conductivity of the duct material was about 50 W/m K. Then a rough estimation of the axial heat conduction may be made as follows:

$$Q_{ac} \cong 50 \times 50 \times 4 \times 0.04 \times 0.002/0.5 = 1.6 \text{ W}.$$

The total power input was in the range from 150 to 250 W. The axial heat conduction was less than about 1%, therefore, the thermal boundary condition may be regarded as uniform heat flux.

A micromanometer with a resolution up to 1.36 Pa was used for pressure drop measurement in the test ducts. The inlet air temperature was measured by a thermocouple checked by a thermometer with a resolution of 0.1 °C. The temperature of the exiting air was measured by five thermocouples distributed at different locations of the outlet cross-section. The thermocouples were calibrated in advance and their accuracy is estimated to be about 0.2 °C. The air flow rate was measured by a rotameter whose accuracy was 2% rated before test. An uncertainty estimation was conducted as suggested by Kline and McClintock (1953). The maximum uncertainty in the average Nusselt number was estimated to be less than 11% and that for the friction factor less than 12%.

## 3. Data reduction

The local heat transfer coefficient was calculated from the total net heat transfer rate and the difference of the local wall temperature and the local bulk mean air temperature

$$h_x = \frac{(Q - Q_{loss})}{A(T_{w,x} - T_{b,x})}. \quad (1)$$

The local wall temperature used in Eq. (1) was read from the output of the thermocouple. The local bulk air temperature of air was calculated by the following equation:

$$T_{b,x} = T_{in} + \frac{(Q - Q_{loss})A(x)}{A\dot{m}c_p}, \quad (2)$$

where $A(x)$ is the heat transfer surface area from the duct inlet to the position where the local heat transfer coefficient was

determined. The heat loss to the environment $Q_{loss}$ was estimated by heat conduction through the plastic foam and the two end losses. For most of the studied values the ratio of $Q_{loss}/Q$ was less than 5%. This estimation was confirmed by the thermal energy balance between the fluid enthalpy increase and the total power input. In the data reduction $Q_{loss}$ was determined from the measured outlet fluid temperature.

The local and the duct average Nusselt numbers were defined by:

$$Nu_x = h_x D_m/k, \tag{3}$$

$$Nu = \frac{(Q - Q_{loss})D_m}{Ak(T_w - T_m)}. \tag{4}$$

The characteristic length, the reference temperature and the average wall temperature were determined by

$$D_m = \frac{D_{h,in} + D_{h,out}}{2},$$
$$T_m = \frac{T_{b,in} + T_{b,out}}{2}, \tag{5}$$
$$T_w = \frac{1}{A}\int_0^A T_{w,x}\,dA.$$

As for most cases of the internal convective heat transfer, the fluid properties are evaluated at the mean temperature of the fluid in the duct (Incropera and DeWitt, 1996).

The Reynolds number was defined by

$$Re_m = \frac{U_m D_m}{v}, \tag{6}$$

where $U_m$ is the duct mean cross-sectional average velocity, which is equal to the cross-section average velocity at the duct mid-section.

The friction factor across the entire duct of the uniform cross-section was defined by

$$f = [(\Delta p/L)D_m)]/(\rho U_m^2/2). \tag{7}$$

For the convergent or divergent duct, the term of pressure drop should be an effective one, which takes the effects of acceleration or deceleration into account (Ward-Smith, 1980). A detailed derivation of the friction factor expression is presented below. Taking a convergent duct as an example (Fig. 6). Let $u$, $v$, $w$ be the velocity components in the $x$, $y$, $z$ directions, $U_{in}$, $U_{out}$ the average axial velocity at inlet and outlet cross-sections, and $A_{in}$, $A_{out}$ the cross-section area of inlet and outlet. Since the variation of the cross-section along the flow direction is not significant, it is assumed that the velocities $v, w$ are very small compared with the mean velocity $U$, and the static pressure is uniform at each cross-section. Then we have

$$\Delta p_e = p_{in} - p_{out} + \frac{1}{2}\rho U_{in}^2 - \frac{1}{2}\rho U_{out}^2, \tag{8}$$

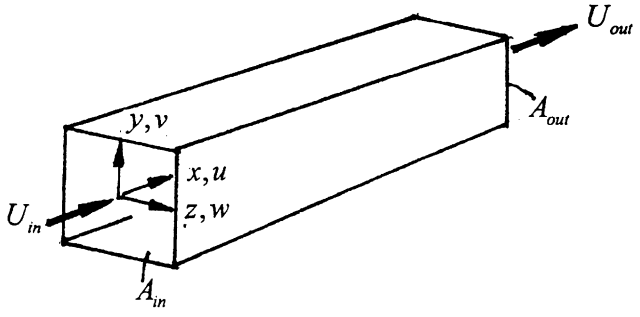


Fig. 6. Diagram for derivation of effective pressure drop.

where $\Delta p_e$ is the effective pressure drop.

The friction factor of the convergent/divergent duct is defined as

$$f = \frac{\Delta p_e}{\rho U_m^2/2}\frac{D_m}{L} = \frac{1}{\rho U_m^2/2}\frac{D_m}{L}\frac{1}{2}\rho U_{in}^2\frac{\Delta p_e}{\rho U_{in}^2/2}. \tag{9}$$

From Eq. (8) we have

$$\frac{\Delta p_e}{\rho U_{in}^2/2} = 1 - \left(\frac{A_{in}}{A_{out}}\right)^2 - \frac{p_{out} - p_{in}}{\rho U_{in}^2/2} = C_{p,i} - C_p, \tag{10}$$

where $C_p$ and $C_{p,i}$ are the pressure recovery factors for viscous fluid and for ideal fluid, respectively

$$C_p = \frac{p_{out} - p_{in}}{\rho U_{in}^2/2}, \quad C_{p,i} = 1 - \left(\frac{A_{in}}{A_{out}}\right)^2. \tag{11}$$

Eq. (10) can be reformulated as

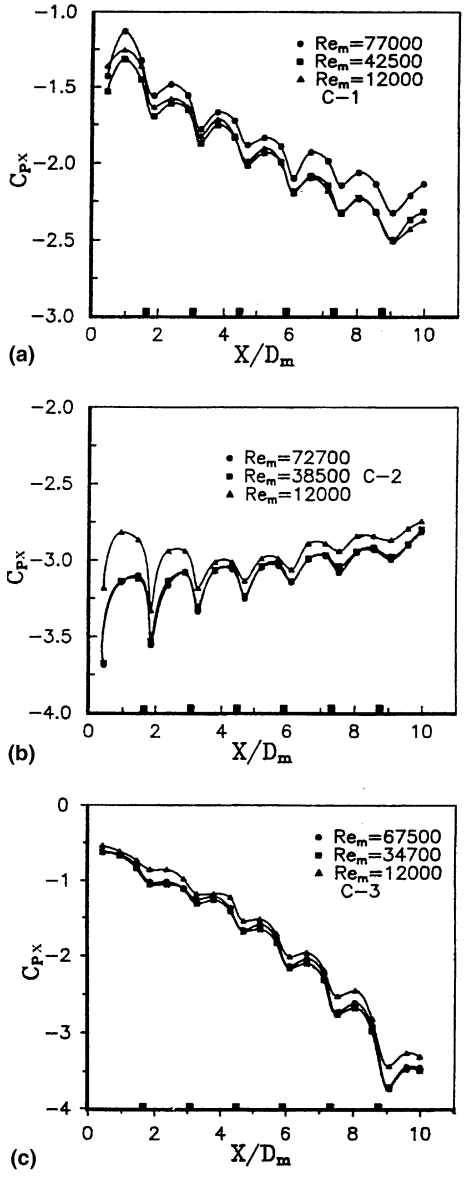


Fig. 7. Local pressure recovery factor.

$$\frac{\Delta p_e}{\rho U_{in}^2/2} = 1 - \left(\frac{A_{in}}{A_{out}}\right)^2 - \frac{p_{out} - p_{in}}{\rho U_{in}^2/2} = C_{p,i}\left(1 - \frac{C_p}{C_{p,i}}\right)$$
$$= \lambda C_{p,i} = \lambda\left[1 - \left(\frac{A_{in}}{A_{out}}\right)^2\right], \quad (12)$$

where $\lambda$ is defined by

$$\lambda = 1 - \frac{C_p}{C_{p,i}}. \quad (13)$$

Then Eq. (9) becomes

$$f = \frac{U_{in}^2}{U_m^2}\frac{D_m}{L}\lambda\left[1 - \left(\frac{A_{in}}{A_{out}}\right)^2\right]. \quad (14)$$

This definition of $C_p$ can be applied for $C_{p,x}$ by replacing $p_{out}$, $p_{in}$ with $p_{x+\Delta x/2}$, $p_{x-\Delta x/2}$, respectively, where $\Delta x$ is the distance between two neighboring pressure taps.

In the tests, the Reynolds number varied from 10 000 to 77 000, and all geometric parameters were kept constant. The values of $e/D_m$ and $p/e$ adopted in this study (0.081, 17.8, respectively) are in the range that has been widely tested for ribbed square ducts with constant cross-section. And the streamwise cross-section variation rate is also close to the reality. Thus the measured results may be regarded as some representative reflecting the effect of the streamwise variation of cross-section on the heat transfer behavior.

## 4. Results and discussion

In order to simplify the presentation, the following symbols are adopted to present the types of ducts: C-1: ribbed uniform cross-section square duct (straight duct); C-2: ribbed divergent duct; and C-3: ribbed convergent duct. In the following, the results for pressure measurements will be presented first, followed by the local and average heat transfer characteristics. Then thermal performance comparison will be conducted between the ribbed duct with constant cross-section and the divergent and convergent ducts.

### 4.1. Pressure distribution

In a periodic ribbed duct as studied here, the streamwise pressure variation also has certain periodic characteristics. The measured local pressure recovery factor is shown in Fig. 7. Six solid square symbols are attached along the abscissa of each figure, representing the streamwise locations of the square rib

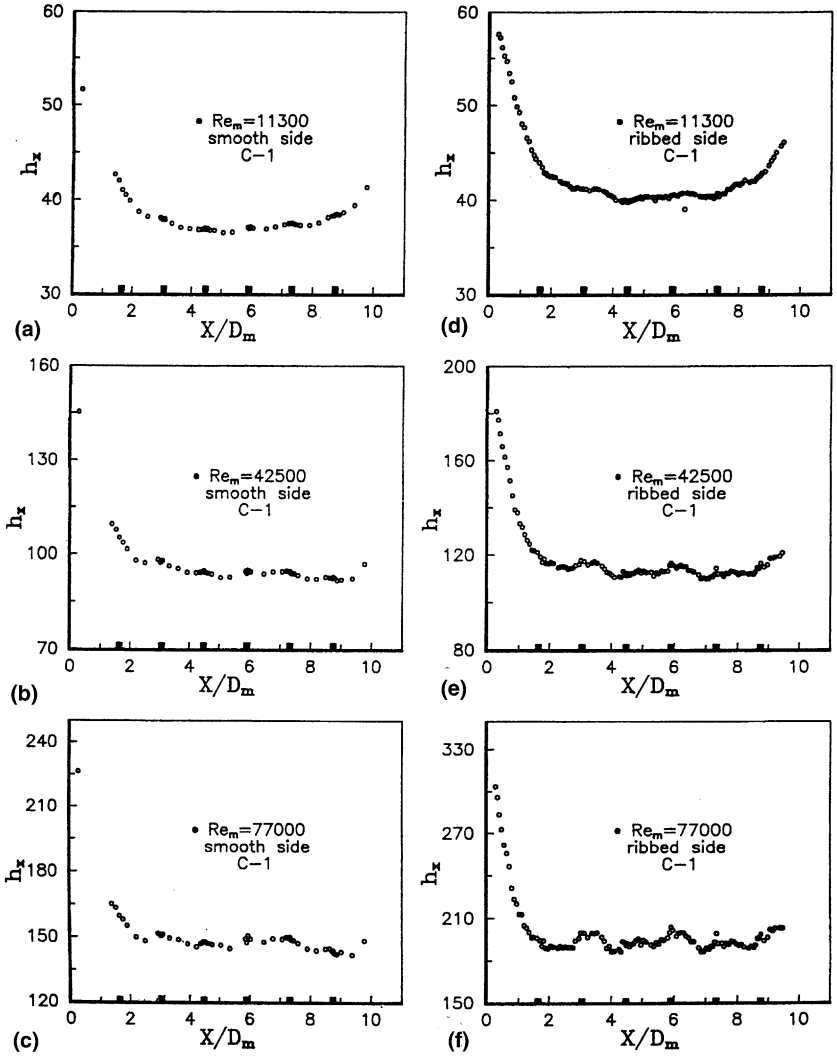


Fig. 8. Local heat transfer coefficient (C-1).

in the test section. Following features may be noted from these experimental results. For all cases, the local pressure distribution initially exhibits an appreciable undulation character, indicating the significant effect of the small rib on the static pressure distribution. For duct C-1, after the second rib the undulation of $C_p$ in one cycle exhibits more or less the same pattern, while for the divergent (C-2) or convergent (C-3) ducts, the amplitude of the undulation keeps decreasing (C-2) or increasing (C-3). These facts imply that for the duct with constant cross-section, the fluid flow may be regarded as periodic fully developed after 2 or 3 cycles, and in the downstream part after the hydrodynamic developing region, the measured centerline pressures for the periodic corresponding positions will fall on a straight line; while for the divergent or convergent ducts there is no such trend. Finally it can be seen that the higher the local velocity, the more appreciable the rib effect on the pressure distribution. This may be attributed to the size of the recirculating zone formed after each rib.

### 4.2. Local heat transfer

The centerline local heat transfer coefficients of the smooth wall and ribbed wall of the ribbed ducts are shown in Figs. 8–10. By a careful examination of these figures we may find the following characteristics: (1) For all the three rib-roughened ducts, the local heat transfer coefficient increases with the increase in the Reynolds number, with the increased rate of duct 1 being the highest. (2) For the ribbed surfaces of the three ducts, the distribution of the local heat transfer coefficient exhibits more or less some periodic pattern after 1–2 ribs. And the higher the Reynolds number, the more significant the periodicity. This is the expected result. However, since the number of thermocouples imbedded to measure the local surface temperatures was limited by some technological reasons indicated in the previous section, the resolution of the local measurement was also restricted. Thus the measured local heat transfer coefficient curve does not possess an ideal periodic pattern, as obtained in Sparrow and Tao (1983), where the naphthalene sublimation technique was used to measure the local mass transfer coefficient for a rod-roughened surface. (3) For the rib-roughened duct of constant cross-section, the heat transfer may be regarded as fully developed after 2–3 ribs, characterizing by almost the same level and variation pattern of the local heat transfer coefficient. It should be noted that for the case of $Re = 11\,300$, the local heat transfer coefficient in the region close to the duct outlet exhibits an in-

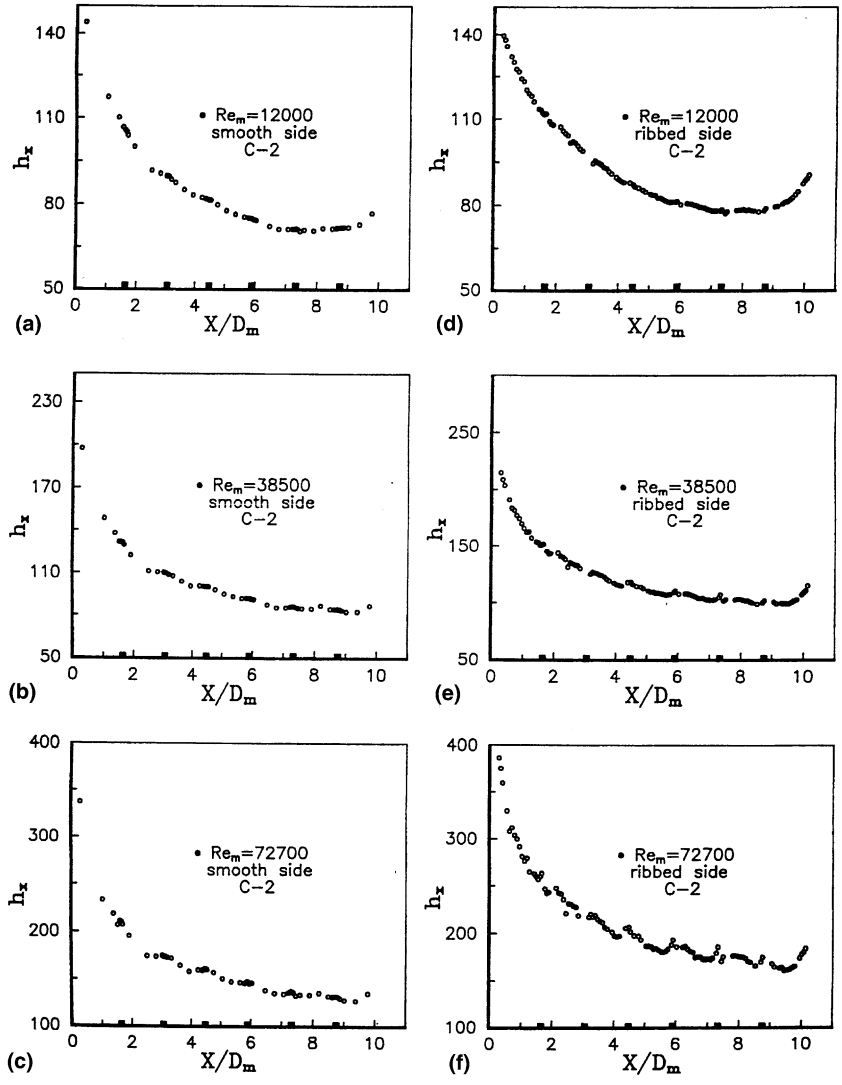


Fig. 9. Local heat transfer coefficient (C-2).

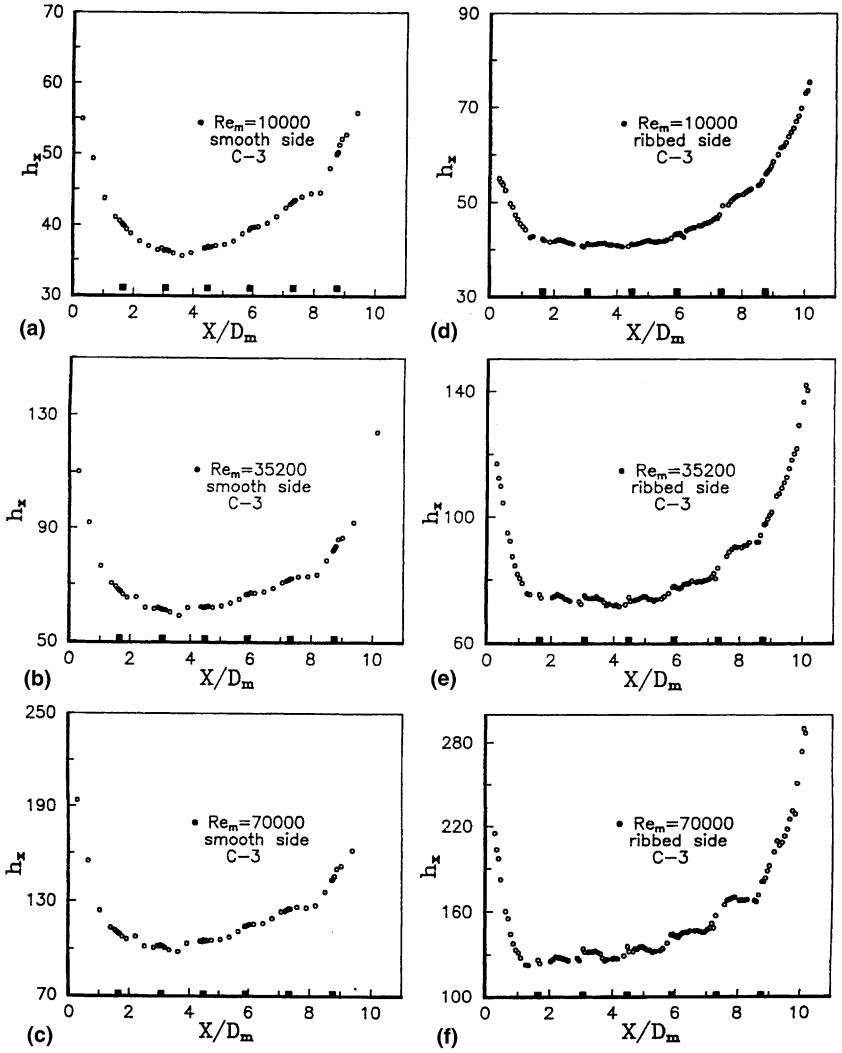


Fig. 10. Local heat transfer coefficient (C-3).

creasing trend. This is expected to have resulted from the end heat loss, which makes the wall temperatures nearby decrease to some extent. The guided-heating method (i.e., an additional heating element was used after the test section to balance the axial heat conduction from the test section) should have been adopted to alleviate such a phenomenon. With the increase of the heat transfer rate, the effect of the end loss decreases, hence, for the other two Reynolds number cases, this increased trend has been significantly alleviated. To present the test results objectively, the data of the last rib for all the three ducts are still retained in the pictures. (4) For the divergent and convergent ducts (C-2 and C-3), there seems no fully developed regime in the downstream region. For the divergent duct, the local heat transfer coefficient keeps continuously decreasing, while for the convergent duct the local heat transfer coefficient keeps continuously increasing. The different streamwise variation patterns of the local heat transfer coefficients of C-2 and C-3 are obviously caused by the streamwise deceleration or acceleration as revealed by previous investigation for two-dimensional boundary layer flows (Succec and Lu, 1990; Tanaka et al., 1982). (5) It is interesting to note that for the smooth surface of the three ducts, the local heat transfer coefficient distribution also exhibits a more or less periodic character for the high Reynolds number cases (see Figs. 9(b) and (c), and 10(b) and (c)). This kind of bouncing-like effect of the rib-roughened surface on the opposing smooth wall was first revealed in Sparrow and Tao (1983). Again, because of the limited number of thermocouples the measured periodic variation pattern of the smooth surface is somewhat vague, but still can be observed. (6) By comparison of the level of the local heat transfer coefficients of the three ducts, it can be seen that at almost the same Reynolds number, the local heat transfer coefficient of the divergent duct (C-2) is the highest, while that of the convergent one (C-3) is the lowest, with that of the constant cross-section duct (C-1) being in between.

### 4.3. Average friction and heat transfer

The Reynolds number dependences of the average friction factor and Nusselt number for the three types of ribbed ducts are shown in Figs. 11 and Fig. 12. In Fig. 11, the ribbed side and smooth side average Nusselt numbers and the duct friction factor are presented, while the average Nusselt numbers for the entire duct are shown in Fig. 12. It can be seen that either the side average or the duct average Nusselt numbers of the three ducts are all higher than what was predicted by the Dittus–Boelter equation. The major reasons accounted for this fact

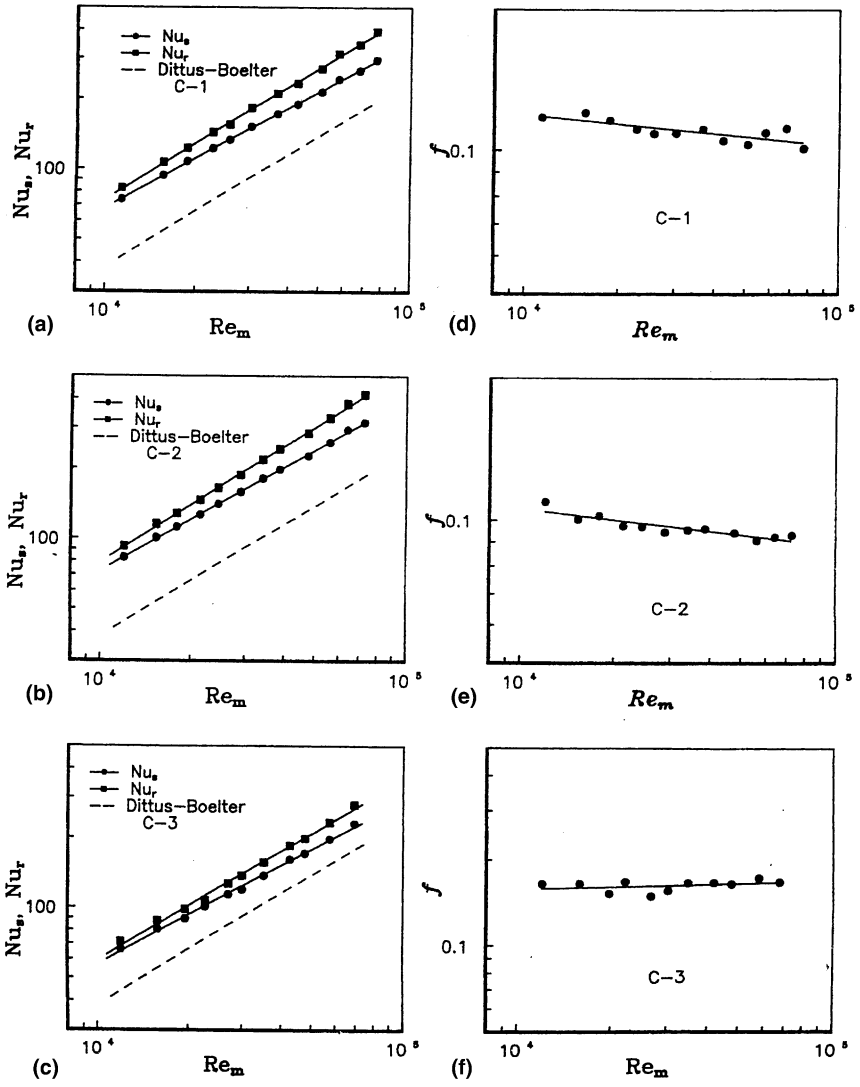


Fig. 11. Friction factor and average Nusselt number of smooth and ribbed sides.

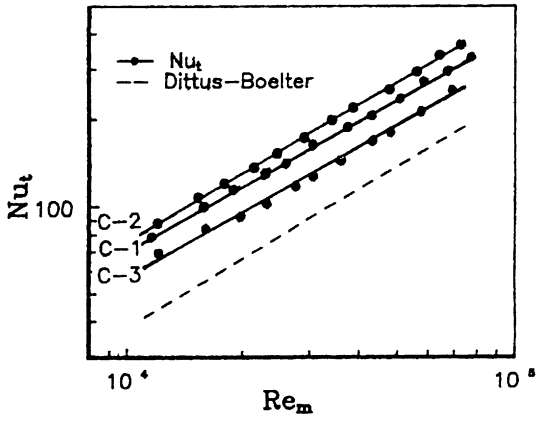


Fig. 12. Duct average Nusselt number.

are: (1) The Dittus–Boelter equation is applied to the fully developed region of a smooth tube, while for the three ducts tested $L/D_m$ is about 12.5, thus for the smooth surface the developing heat transfer rather than the developed one is dominated; (2) The heat transfer of a ribbed surface is enhanced by the existence of ribs which act as turbulent promoters, and these ribs also can improve the heat transfer at the smooth surfaces. It is to be noted that the difference between Nusselt numbers of the smooth side and ribbed side increases with the increase in $Re_m$. The Reynolds number dependency of friction factor for the C-1 and C-2 ducts exhibits the conventional character: friction factor decreases with the increase in Reynolds number. However, for the convergent duct (C-3), the variation trend is the opposite. This is because in the convergent duct the cross-sectional area decreases along the flow direction, leading to an ever-increasing blockage effect of the rib on the fluid flow characteristics.

### 4.4. Heat transfer performance comparison

Attention is now turned to the relative performance of the different ribbed ducts. The three widely used constraints for thermal performance comparison are adopted: identical flow rate, identical pumping power, and identical pressure drop. Based on the constant property assumption and the same characteristic length, the formulations of the three constraints are given in the following:

(a) *Identical mass flow rate*:

$$(\dot{m})^* = \dot{m}, \tag{15a}$$

where the superscript "$*$" stands for the compared duct and the quantity without $*$ for the reference duct. From Eq. (15a) we can obtain the following relationship between the Reynolds number of the duct compared and the reference duct

$$Re_m^* = Re_{\mathrm{m}}(D_{\mathrm{m}}^*/D_{\mathrm{m}})(A/A^*). \tag{15b}$$

For the three cases compared, $D_{\mathrm{m}}^*/D_{\mathrm{m}} = 1$, and $A/A^* = 1$. To make the expression more general, these two terms are kept as it is.

(b) *Identical pumping power*:

$$\left(\frac{\dot{m}}{\rho}\Delta p\right)^* = \left(\frac{\dot{m}}{\rho}\Delta p\right). \tag{16a}$$

This leads to

$$Re_{\mathrm{m}}^* = \sqrt[3]{\frac{Af\,Re_{\mathrm{m}}^3}{(Af)^*}}. \tag{16b}$$

(c) *Identical pressure drop*:

$$(fU^2)^* = fU^2. \tag{17a}$$

Then we have

$$Re_m^* = Re_{\mathrm{m}}\sqrt{f/f^*}. \tag{17b}$$

Under the condition of same temperature difference between the fluid and the wall, the ratio of heat transfer between the compared duct and the reference duct may be formulated as follows:

$$\frac{Q^*}{Q} = \frac{[ANu(Re_{\mathrm{m}})]^*}{ANu(Re_{\mathrm{m}})}, \tag{18}$$

where $Nu(Re_{\mathrm{m}})$ represents the experimental correlation between the Nusselt number and the Reynolds number.

The comparisons of the duct average heat transfer performance for the three ribbed ducts are shown in Fig. 13, where the ratio of heat transfer rate in two ducts are presented. For example, the symbol C-2:C-1 indicates the ratio of heat transfer rate of C-2 over that of C-1. It can be seen from Fig. 13(a) that in the identical mass flow rate, the heat transfer enhancement is about 10–16% and −17% to −20% for the ribbed divergent duct and convergent duct, respectively, compared with the ribbed duct of constant cross-section. From Fig. 13(b) it can be observed that in the identical pumping power, the heat transfer enhancement is about 10–20% and −25% to −30% for the ribbed divergent duct and convergent duct, respectively, compared with duct C-1. Fig. 13(c) shows that in the identical pressure drop, the heat transfer enhancement is about 10–25% and −25% to −32% for the ribbed divergent duct and convergent duct, respectively, compared with duct C-1. It is to be noted that under the identical mass flow rate condition, $Re_{\mathrm{m}}^* = Re_{\mathrm{m}}$, and both ducts C-1 and C-3 show enhanced heat transfer when compared with the Dittus–Boelter equation. However, the enhancement percentage of duct C-1 is much larger than that of C-3. Thus the ratio of heat transfer rate of C-3 over that of C-1 is less than unity.

The above comparison definitely shows that for the three ribbed square ducts, the divergent duct has the highest heat transfer performance, while the convergent ducts behave the worst, with the duct C-1 being somewhat in between. Following considerations may account for such results. First, as indicated in Succec and Lu (1990), Tanaka et al. (1982), streamwise acceleration may lead to a thermal boundary layer penetrating significantly beyond the hydrodynamic boundary layer. Thus the thermal resistance of the convective heat transfer between the main stream and the surface increases. On the opposite, the streamwise deceleration causes the thermal boundary layer thickness to be less than the hydrodynamic boundary layer, leading to an enhancement of the heat transfer. It is interesting to note that this streamwise acceleration or deceleration has especially a profound effect on the local heat transfer in the entrance region, where for all the three ducts, the local heat transfer coefficient is the highest in the entire duct. For the divergent duct the local heat transfer coefficient in the inlet region is very high, while the local heat transfer coefficient in the inlet region of the convergent duct is only about half or even less than that of the divergent duct.

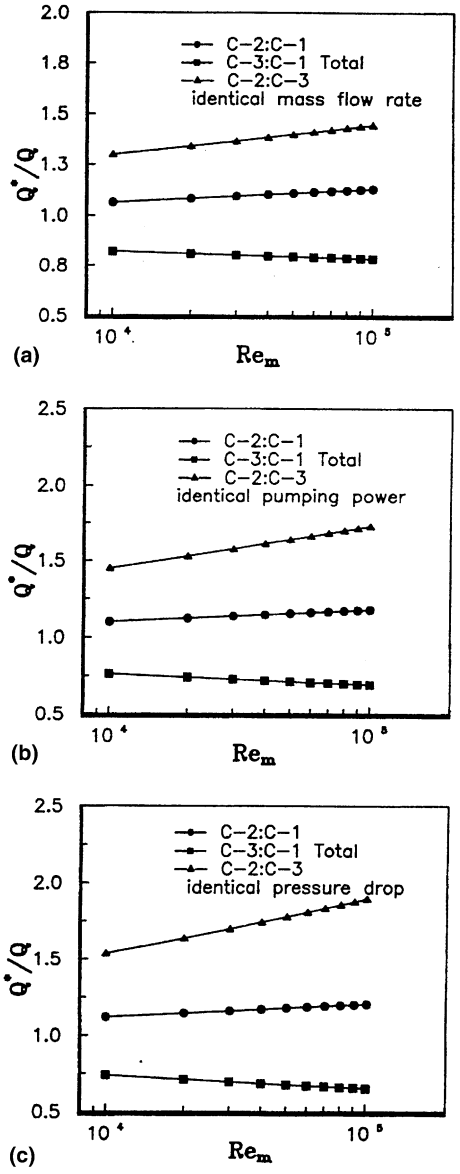


Fig. 13. Heat transfer performance comparison.

## 5. Concluding remarks

The work reported here is a systematic experimental study of the three ribbed square ducts (ribbed duct with constant cross-section, ribbed divergent square duct and ribbed con-

vergent square duct). The local heat transfer coefficient and pressure recovery factor distribution, the average Nusselt number and friction factor are presented. The heat transfer enhancement comparisons are made with ribbed straight duct as a reference under the constraints of identical mass flow rate, identical pumping power and identical pressure drop. One unique feature is that the purpose of the present test model is to investigate the departure of the simulation of the actual blade inter-cooling passage with the straight and rectangular without considering the divergent and convergent ducts along the flow direction.

Because of the streamwise flow acceleration and deceleration, the local heat transfer and pressure recovery factor characteristics of the three types of ducts are very different. The local heat transfer coefficient decreases continuously in the streamwise direction in the ribbed divergent duct. For the ribbed convergent duct the local heat transfer coefficient decreases rapidly at the inlet region, and then soon increases rapidly along the main flow direction. Both axial distribution of the local heat transfer coefficients and pressure recovery factor reveal that the periodic fully developed regime in the ribbed constant cross-section duct has been established after 2–3 ribs. While for the ribbed divergent duct and convergent duct, there seems no such a fully developed region.

Under the three constraints of comparison (identical mass flow rate, pumping power and pressure drop), the ribbed divergent duct has the largest heat transfer rate, while heat transfer in the ribbed convergent duct is deteriorated compared to the ribbed square duct of constant cross-section. The main reason for this phenomenon may be attributed to the streamwise acceleration (convergent duct) or deceleration (divergent duct), which changes the relative thickness of the thermal boundary layer to the hydrodynamic boundary layer.

## Acknowledgements

This work was supported by the National Key Project of Fundamental R&D of China (Grant No. G2000026303) and the National Natural Science Foundation of China (No. 59806011). The authors are also grateful to the three reviewers for their valuable suggestions and comments.

## References

Abuaf, N., Kercher, D.M., 1994. Heat transfer and turbulence in a turbine blade cooling circuit. ASME J. Turbomachinery 116, 169–177.

Burggraf, F., 1970. Experimental heat transfer and pressure drop with two-dimensional discrete turbulent promoters applied to two opposite walls of a square tube. Bergles, A.E., Webb, R.L. (Eds.), Augmentation of Convective Heat and Mass Transfer. ASME, New York, pp. 70–79.

Chyu, M.K., Naturajan, V., 1995. Surface heat transfer from a three-pass blade cooling passage simulator. ASME J. Heat Transfer 117, 650–656.

Han, J.C., 1984. Heat transfer and friction in channels with two opposite rib-roughened walls. ASME J. Heat Transfer, 774–781.

Han, J.C., Glicksman, L.R., Rohsenow, W.M., 1978. An investigation of heat transfer and friction for rib-roughened surfaces. Int. J. Heat Mass Transfer 21, 1143–1156.

Han, J.C., Lei, C.K., 1983. Heat transfer and friction in square ducts with two opposite rib-roughened surfaces. ASME Paper No. 83-HT-26.

Han, J.C., Park, J.S., 1988. Developing heat transfer in rectangular channels with rib turbulators. Int. J. Heat Mass Transfer 31, 183–195.

Han, J.C., Park, J.S., 1998. Developing heat transfer in rectangular channels with rib turbulators. Int. J. Heat Mass Transfer 31, 183–195.

Han, J.C., Park, J.S., Lei, C.K., 1985. Heat transfer enhancement in channels with turbulence promoters. ASME J. Eng. Gas Turbines Power 107, 628–635.

Incropera, F.P., DeWitt, D.P., 1996. Introduction to Heat Transfer, third ed. Wiley, New York, pp. 412–413.

Kline, S.J., McClintock, F.A., 1953. Describing uncertainties in single-sample experiments. Mech. Eng. 75, 3–8.

Lau, S.C., McMillin, R.D., Han, J.C., 1991. Turbulent heat transfer and friction in a square channel with discrete rib turbulators. ASME J. Turbomachinery 113, 360–366.

Liou, T.M., Hwang, J.J., Chen, S.H., 1993. Simulation and measurement of enhanced turbulent heat transfer in channel with periodic rib on one principle wall. Int. J. Heat Mass Transfer 36, 507–517.

Lockett, J.F., Collins, M.W., 1990. Holographic interferometry applied to rib-roughness heat transfer in turbulent flow. Int. J. Heat Mass Transfer 33 (11), 2439–2449.

Medwell, J.O, Morris, W.D., Xia, J.Y., Taylor, C., 1991. An investigation of convective heat transfer in a rotating coolant channel. ASME J. Turbomachinery 113, 354–359.

Metzger, D.E., Fan, C.S., Pennington, J.W., 1998. Heat transfer and flow characteristics of very rough transverse ribbed surfaces with and without pin fins. Proc. ASME-JSME Thermal Eng. Joint Conf. 1, 429–436.

Metzger, D.E., Fan, C.S., Plevich, C.W., 1998. Effects of transverse rib roughness on heat transfer and pressure losses in rectangular ducts with sharp 180 degree turns. Paper AIAA-88-0166.

Miller, R.W., 1996. Flow Measurement Engineering Handbook, third ed. McGraw-Hill, New York.

Sparrow, E.M., Tao, W.Q., 1984. Symmetric vs asymmetric periodic disturbances at the walls of a heated flow passage. Int J. Heat Mass Transfer 27 (11), 2133–2144.

Sparrow, E.M., Tao, W.Q., 1983. Enhanced heat transfer in a flat rectangular duct with streamwise periodic disturbances at one principle wall. ASME J. Heat Transfer 105, 851–861.

Succec, J., Lu, Y., 1990. Heat transfer across turbulent boundary layers with pressure gradients. ASME J. Heat Transfer 112, 906–912.

Tanaka, H., Kawamura, H., Tateno, A., Hatamaya, S., 1982. Effects of laminarization and retransition on heat transfer for low Reynolds number flow through a converging to a constant area. ASME J. Heat Transfer 104, 363–370.

Taslim, M.E., Spring, S.D., 1987. Friction factors and heat transfer coefficients in turbulated passages of different aspect ratios. Part I. Experimental results. Paper No. AIAA-87-2009.

Taslim, M.E., Spring, S.D., 1988. Experimental heat transfer and friction factors in turbulated cooling passages of different aspect ratios where turbulators are staggered. Paper No. AIAA-88-3014.

Taslim, M.E., Spring, S.D., 1991. An experimental investigation into the effects of turbulator profile and spacing on heat transfer coefficients and friction factors in small cooled turbine airfoils. Paper No. AIAA-91-2033.

Wang, L.B., Wang, Q.W., He, Y.L., Tao, W.Q., 2001. Experimental and numerical study of developing turbulent flow and heat transfer in convergent and divergent square ducts. J. Heat Mass Transfer (in press).

Ward-Smith, A.J., 1980. Internal Fluid Flow. Oxford University Press, Oxford, pp. 195–247.